Journal of Power Sources 261 (2014) 324–331

Contents lists available at ScienceDirect

Journal of Power Sources

journal homepage: www.elsevier.com/locate/jpowsour

A new route for the synthesis of Li_2MnO_3 based cathode material with enhanced first cycle efficiency and cycleability for lithium ion batteries

Wenwen Zhao [a], Shuji Harada [a], Yasuyuki Furuya [a], Shinji Yamamoto [b], Hideyuki Noguchi [a,*]

[a] Department of Advanced Technology Fusion, Graduate School of Science and Engineering, Saga University, Honjo-1, Saga 840-8520, Japan
[b] Nissan Research Center, Nissan Motor Co., Ltd., Natsushima-cho, Yokosuka, Kanagawa 237-8523, Japan

HIGHLIGHTS

- $Li_xNi_{1/3}Mn_{2/3}O_2$ ($x > 2/3$) was synthesized via a new reduction-ion exchange method.
- $Li_xNi_{1/3}Mn_{2/3}O_2$ ($x > 2/3$) shows similar features as those of Li_2MnO_3 based cathode.
- $Li_xNi_{1/3}Mn_{2/3}O_2$ ($x > 2/3$) delivers enhanced first cycle efficiency and cycleability.
- Mg substituted compound, $Li_xNi_{2/9}Mg_{1/9}Mn_{2/3}O_2$, exhibits improved cycleability.

ARTICLE INFO

Article history:
Received 4 January 2014
Received in revised form
21 February 2014
Accepted 6 March 2014
Available online 26 March 2014

Keywords:
Lithium ion battery
Li excess cathode
Reduction-ion exchange
Electrochemical performance
Improved cycleability

ABSTRACT

$Li_xNi_{1/3}Mn_{2/3}O_2$ ($x > 2/3$) compounds have been synthesized from P3 type $Na_{2/3}Ni_{1/3}Mn_{2/3}O_2$ precursor through a new reduction-ion exchange method. The XRD patterns of $Li_xNi_{1/3}Mn_{2/3}O_2$ show superlattice peak around $2\theta = 20°$, which is similar to that of the lithium-excess manganese based cathode materials. In contrast to sample obtained from traditional ion exchange method, the $Li_xNi_{1/3}Mn_{2/3}O_2$ compound delivers $LiNi_{1/2}Mn_{1/2}O_2$–Li_2MnO_3 solid solution type potential profiles and higher capacity than that of $Li_{2/3}Ni_{1/3}Mn_{2/3}O_2$, especially for the capacity delivered in high potential region. Moreover, it exhibits extremely small irreversible capacity at the initial cycle and small capacity loss during cycling in the voltage range 4.7–2.5 V. The structure and electrochemical properties of metallic elements substituted $Li_xNi_{2/9}M_{1/9}Mn_{2/3}O_2$ (M = Al, Co, Fe, Mg) were also studied. XRD and Raman spectra results suggest that small amount substitution of Ni with other metal ions does not affect the main structure of $Li_xNi_{2/9}M_{1/9}Mn_{2/3}O_2$ compounds. For Mg substituted compound, $Li_xNi_{2/9}Mg_{1/9}Mn_{2/3}O_2$, it exhibits improved cycleability compared with the other samples.

1. Introduction

Lithium manganese oxide based cathode materials have been studied intensively as cathode material for Lithium ion battery due to the abundance, lower cost and environmental benign of manganese [1–7]. Various Mn based derivatives such as layered $LiMnO_2$ [1,2], spinel $LiMn_2O_4$ [3,4] and $Li_{0.44}MnO_2$ [5–7] have caught the eyes of many researchers in the past several years. Owing to the difference in structure, those materials show different electrochemical properties. Layered $LiMnO_2$ is proved to be hard to prepare via traditional solid state method due to the formation of monoclinic phase [2]. Therefore, ion exchange of $NaMnO_2$ in Li salt has been employed for the synthesis of $LiMnO_2$ with stable electrochemical property [8,9]. Though $LiMnO_2$ synthesized from the above method showed relatively high capacity, it also undergoes capacity fading upon cycling and transformation to spinel structure [10]. The recently developed Li excess manganese oxides, noted as $xLiMO_2$–$(1-x)Li_2MnO_3$ (M = Ni, Co, Fe, Ti), have attracted a great attention of many researchers due to their excellent properties in terms of high specific capacity and high working potential [11–14]. Despite the above properties, these materials suffer from some problems such as low first cycle efficiency, unstable cyclability and structure transformation during prolonged cycling. Consequently, further studies are necessary to circumvent the above issues.

The structure and electrochemical properties of AMO_2 (A: alkali metal, M: transition metal) bronzes with various structures such as P3, P2, O3 and O2 have been systematically studied by Delmas group [15–17]. Here, the letters P, O represent the alkali

* Corresponding author. Tel.: +81 952 28 8674; fax: +81 952 28 8591.
E-mail address: noguchih@cc.saga-u.ac.jp (H. Noguchi).

http://dx.doi.org/10.1016/j.jpowsour.2014.03.069
0378-7753/

environmental (prismatic and octahedral) and the numbers show the MO_2 sheets in per unit cell. A series of Mn-based oxides, $Li_{2/3}Ni_{1/3}Mn_{2/3}O_2$, possessing layered structure have been investigated by Paulsen et al. [18–21]. They have shown that $Li_{2/3}Ni_{1/3}Mn_{2/3}O_2$ can possess O2, O3, or T2 structure depending on the Na containing precursors and ion exchange conditions. $Na_{2/3}Ni_{1/3}Mn_{2/3}O_2$ with P3 structure can be used as precursor to synthesize O3 $Li_{2/3}Ni_{1/3}Mn_{2/3}O_2$ through ion exchange reaction in LiCl–$LiNO_3$ molten salt. $Li_{2/3}Ni_{1/3}Mn_{2/3}O_2$ prepared from traditional ion exchange method show good electrochemical performance. However, the first charge capacity is around 120 mAh g^{-1} in the voltage range 2.5–4.6 V since roughly 1/3 mol Li can be extracted from the lattice during the first charge process. In the following cycles, the reversible insertion and extraction of 2/3 mol Li in $Li_{2/3}Ni_{1/3}Mn_{2/3}O_2$ result in a capacity about 200 mAh g^{-1}. Another issue for $Li_{2/3}Ni_{1/3}Mn_{2/3}O_2$ is that the structure transformation from O3 to spinel like phase occurs during cycling. This has also been reported for Li excess manganese oxide cathode [22]. Another common feature between O3 $Li_{2/3}Ni_{1/3}Mn_{2/3}O_2$ type and Li excess manganese oxide is that both of them show hysteresis in the charge–discharge profile. The above features of two cathodes inspire us to explore the possibility of preparing Li excess manganese oxide from P3 type $Na_{2/3}Ni_{1/3}Mn_{2/3}O_2$.

In $Na_{2/3}Ni_{1/3}Mn_{2/3}O_2$, it is clear that Mn is in tetravalent state and it is possible that Mn^{4+} could be partially reduced to Mn^{3+} thus to incorporate more Li into the matrix. The use of LiI as reducing agent to incorporate extra to the host structure has been reported before [23,24]. Herein, in this study, simultaneous reduction and lithium exchange in molten salts consisting $LiNO_3$ and LiI was employed to achieve this goal. By using this method, extra lithium can be incorporated into the P3 precursor to form $Li_xNi_{1/3}Mn_{2/3}O_2$ ($x > 2/3$). The structure and electrochemical properties of the as-prepared $Li_xNi_{1/3}Mn_{2/3}O_2$ have been evaluated. The effect of metallic elements substitution on the properties of the as-prepared $Li_xNi_{1/3}Mn_{2/3}O_2$ compound has also been investigated.

2. Experimental

2.1. Synthesis of $Na_{2/3}Ni_{1/3}Mn_{2/3}O_2$

Solid state method was used for the synthesis of $Li_xNi_{1/3}Mn_{2/3}O_2$. The precursor P3 $Na_{2/3}Ni_{1/3}Mn_{2/3}O_2$ was prepared through a simple combustion method. Typically, stoichiometric amounts of nickel nitrate ($Ni(NO_3)_2$), manganese nitrate ($Mn(NO_3)_2$) and sodium nitrate ($NaNO_3$) were mixed in triethyleneglycol. The mixture was fired at around 400 °C and ash like powder can been obtained after the vigorous combustion of organic materials. The decomposed powder was ball-milled for 1 h and was subsequently calcinated at 700 °C in air for 10 h to form P3 type $Na_{2/3}Ni_{1/3}Mn_{2/3}O_2$ precursor. The obtained dark black compound was ground to fine powder for ion exchange. For the synthesis of P3 $Na_{2/3}Ni_{2/9}M_{1/9}Mn_{2/3}O_2$ (M = Al, Co, Fe, Mg) precursors, similar procedure was used.

2.2. Synthesis of $Li_{2/3}Ni_{1/3}Mn_{2/3}O_2$ and $Li_xNi_{1/3}Mn_{2/3}O_2$

The as prepared P3 $Na_{2/3}Ni_{1/3}Mn_{2/3}O_2$ was used to synthesize $Li_{2/3}Ni_{1/3}Mn_{2/3}O_2$ through normal ion exchange method as reported before [20]. Typically, $Na_{2/3}Ni_{1/3}Mn_{2/3}O_2$ was mixed with $LiNO_3$ and LiCl and ground for ion exchange. The molar ratio of Li ion to Na ion was approximately 5:1. After soaking in the melt for 6 h, the mixture was left to cool to room temperature. After the product was washed with hot water, filtered and dried, black power was obtained.

Reduction-ion exchange was done by using the molten salt composed of $LiNO_3$ and LiI at 280 °C in air for 6 h. During the ion exchange, purple I_2 gas evolution was observed, which indicates the reduction of metal ions has evolved. After the melt was allowed to cool to room temperature, the mixture was washed with hot water to remove the residual lithium salt. Then, it was filtered and the recovered powder was dried at 80 °C for 12 h. The desired compounds turned to be in reddish powder.

2.3. Instrumentation

The structure of the compounds was characterized by powder X-ray diffraction measurement (XRD) for two theta value from 10° to 80° (CuKα radiation, XRD-7000, SHIMADZU). Induced coupled plasma (ICP) was used to determine the composition of the obtained compounds. Nitrogen adsorption–desorption isotherm were carried out after the samples were outgassed and dehydrated at 200 °C for 24 h (Micromeritics Gemini 2360, SHIMADZU). The specific surface area of each sample was calculated from the Brunauer–Emmett–Teller (BET) method. The morphology of the compounds was observed by Scanning Electron Microscope (SEM, JEOL, JSM-5200) and Transmission Electron Microscope (TEM, JEOL, JEM-1210). Fourier transform infrared spectroscopy (FTIR) spectra of the samples were performed on a JASCO 400 FTIR spectrometer. Samples were mixed with KBr and pressed to form pellets for measurement. Raman measurements were made with a spectrometer as reported in previous studies with some modifications [25,26]. The Raman spectra were measured by SpectraPro 2300i imaging spectrograph (Princeton Instruments, New Jersey) equipped with a liquid nitrogen cooled charge-coupled device (Spec-10:256E, Roper Scientific). All samples were excited with the 532 nm light available from a diode-pumped solid-state laser (Ventus532, Laser Quantum, Cheshire, UK), and a back scattered light was collected by collection optics. A long wave path edge filter (LP03-532RS-25, Semrock) was used to eliminate the intense Rayleigh light. All the spectra were taken at room temperature, and homemade software eliminated the noise spikes in the spectra caused by cosmic rays.

2.4. Electrochemical characterization

CR2032 type coin cells were assembled to evaluate the electrochemical properties of the obtained compounds. Lithium foil was used as the anode and glass fiber filter with a thickness of 100 μm was used as the separator (GA-100, made by ADVANTEC). For the fabrication of working electrodes, 20 mg active material together with 10 mg conducting binder (Teflon:acetylene black = 1:2) was mixed and pressed on the stainless steel mesh. Then, the electrodes were dehydrated by a vacuum dry at 180 °C for 6 h. The electrolyte used was 1 M lithium phosphorus hexafluoride ($LiPF_6$) in a mixture of ethylene carbonate (EC) and dimethyl carbonate with (DMC) volume ratio of 1:2. The cells were assembled in a glove box filled with pure argon gas. The assembled cells were cycled at a current density of 20 mA g^{-1} (0.1 C rate) between 2.5 and 4.7 V at 50 °C.

3. Results and discussion

3.1. Characterization of $Li_xNi_{1/3}Mn_{2/3}O_2$

Fig. 1 shows the XRD patterns of P3 precursor $Na_{2/3}Ni_{1/3}Mn_{2/3}O_2$, normal ion exchanged product, $Li_{2/3}Ni_{1/3}Mn_{2/3}O_2$ and reduction-ion exchange sample, $Li_xNi_{1/3}Mn_{2/3}O_2$. All peaks in the XRD patterns of $Na_{2/3}Ni_{1/3}Mn_{2/3}O_2$ can be indexed to P3 layer structure with the space group of R3m. No impurities were observed for P3 precursor. For $Li_{2/3}Ni_{1/3}Mn_{2/3}O_2$, all the peaks are indexed to a $NaFeO_2$ structure with the space group of $R\bar{3}m$. Also,

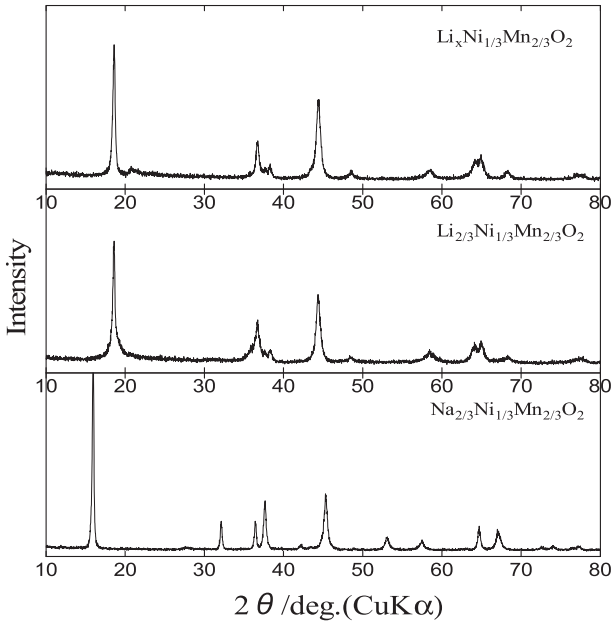

Fig. 1. XRD patterns of P3 precursor, normal ion exchanged $Li_{2/3}Ni_{1/3}Mn_{2/3}O_2$ and $Li_xNi_{1/3}Mn_{2/3}O_2$.

the strong peak located at $2\theta = 16°$ in precursor shifts to high angle indicating the exchange of Na with Li ions. The splitting of peaks at $2\theta = 64°$ also reveals the well-defined layer structure of the ion exchanged samples. In the case of $Li_xNi_{1/3}Mn_{2/3}O_2$, except for the peaks at $2\theta = 22°$, it shows almost same XRD patterns as that of $Li_{2/3}Ni_{1/3}Mn_{2/3}O_2$. The peaks located at $2\theta = 22°$ may be attributed to the super-lattice ordering of Li and Mn in the transition layers, since such superlattice peaks are observed for Li-excess based materials.

For normal ion exchange samples carried out in $LiNO_3$ and LiCl molten salt system, there is no observation of the superlattice peaks in the XRD patterns since only 2/3 mol Li can be exchanged with Na. However, for the samples ion exchanged under the system of $LiNO_3$ and LiI molten salt, one can expect that extra Li can be incorporated in $Na_{2/3}Ni_{1/3}Mn_{2/3}O_2$ due to the strong reduction ability of LiI. Li content for all the ion exchanged samples conducted by ICP measurement is shown in Table 1. From the ICP results it is clear that the Li content extends to more than 1.0 mol for $Li_xNi_{1/3}Mn_{2/3}O_2$, which demonstrates that extra Li can be incorporated in $Na_{2/3}Ni_{1/3}Mn_{2/3}O_2$ to form lithium excess phase. Furthermore, the decreasing of Mn oxidation state was also confirmed for $Li_xNi_{1/3}Mn_{2/3}O_2$, which implies that Mn is partially reduced to lower oxidation state by LiI. The use of LiI as reducing agent to incorporate extra Li into P2 $Na_{2/3}Ni_{1/3}Mn_{2/3}O_2$ has been reported by Shaju et al. [27]. They have demonstrated that utilization of LiI is effective to obtain O2 $LiNi_{1/3}Mn_{2/3}O_2$ with partially Mn in trivalent state.

In order to investigate the morphology of the samples, the SEM measurement was carried out. Fig. 2 shows the SEM images of P3 $Na_{2/3}Ni_{1/3}Mn_{2/3}O_2$, $Li_{2/3}Ni_{1/3}Mn_{2/3}O_2$ and $Li_xNi_{1/3}Mn_{2/3}O_2$. The average particle size of $Na_{2/3}Ni_{1/3}Mn_{2/3}O_2$ precursor is around 15–20 μm. $Li_{2/3}Ni_{1/3}Mn_{2/3}O_2$ and $Li_xNi_{1/3}Mn_{2/3}O_2$ seemed to have similar particle size. From the larger magnification SEM images it is obvious to see that the aggregation of particle occurred in three samples, which is common for samples prepared by solid state method. Therefore, further optimization of synthesis method, such as co-precipitation method, would be an effective to reduce the secondary particle size as well as particles with uniform morphology. BET data listed in Table 1 indicated that the surface area of ion exchanged samples increased compared with that of P3 precursor.

Table 1
Composition and surface area of P3 precursor and ion exchange samples.

Intended composition	Observed composition	Surface area BET ($m^2\ g^{-1}$)
$Na_{2/3}Ni_{1/3}Mn_{2/3}O_2$	$Na_{0.663}Ni_{0.324}Mn_{0.676}O_{2+\delta}$	5.7
$Li_{2/3}Ni_{1/3}Mn_{2/3}O_2$	$Li_{0.652}Ni_{0.328}Mn_{0.672}O_{2+\delta}$	6.3
$LiNi_{1/3}Mn_{2/3}O_2$	$Li_{1.25}Ni_{0.326}Mn_{0.670}O_{2+\delta}$	8.6

Vibrational spectroscopy such as Fourier transform infrared (FTIR) and Raman scattering, are strong techniques sensitive to the short range environment of oxygen coordination around the cations in oxide lattices [28]. It is believed the above techniques are proper for the solving the problems of phase determination when various cationic environments are present. FTIR spectra have been employed in the determination of the local environment of the cations and the host matrix of cathode materials for LIBs [29]. The IR spectra of P3 precursors and the ion exchanged samples are presented in Fig. 3. For comparison, the FTIR spectrum of Li_2MnO_3 was also presented. In the spectrum of $Na_{2/3}Ni_{1/3}Mn_{2/3}O_2$, there are mainly three bands can be observed. A broad shoulder around 620 cm^{-1}, a strong band located at 520 cm^{-1} and small sharp band at 450 cm^{-1}. These three IR active modes assigned to the stretching and bending vibrations of octahedrally coordinated molecule of MO_6 in $Na_{2/3}Ni_{1/3}Mn_{2/3}O_2$ matrix. In the case of normal ion exchanged sample, $Li_{2/3}Ni_{1/3}Mn_{2/3}O_2$, the sharp bands at 420 cm^{-1} become broad and shoulder at 620 cm^{-1} is noticeable. There is no obvious shift in the band position of main strong band at 520 cm^{-1}. The FTIR spectrum of $Li_xNi_{1/3}Mn_{2/3}O_2$ is different from that of $Li_{2/3}Ni_{1/3}Mn_{2/3}O_2$. The strong band at 520 cm^{-1} shifts towards high frequency and band at 620 cm^{-1} is barely noticeable. Such a change in the FTIR spectrum can be attributed to the incorporation of extra lithium ion into $Li_{2/3}Ni_{1/3}Mn_{2/3}O_2$ which results in difference in the local environment of the cations. In comparison with the FTIR spectrum of Li_2MnO_3, $Li_xNi_{1/3}Mn_{2/3}O_2$ shows similar FTIR features, which indicates the similar cationic environment might exist in $Li_xNi_{1/3}Mn_{2/3}O_2$ matrix.

Raman spectroscopy was carried out for the samples to further investigate the local cation configuration. Fig. 4 shows the Raman spectra of the precursors and their ion exchanged samples. The Raman spectrum of $Na_{2/3}Ni_{1/3}Mn_{2/3}O_2$ contains four sharp peaks, which are located at 349, 394, 482, 593 cm^{-1}. Also, a broad peak at 637 cm^{-1} can be observed. The Raman spectra of ion exchanged samples are quite different from those of precursors. Two prominent peaks located at 484 and 605 cm^{-1} can only be detected for $Li_{2/3}Ni_{1/3}Mn_{2/3}O_2$. In comparison with the Raman spectrum of $Na_{2/3}Ni_{1/3}Mn_{2/3}O_2$, one can see that there are peak shifts toward the high frequency side. Furthermore, peaks intensity reversed after ion exchange. Such change in peak position and peak intensity would be due to the different chemical bond environmental for the samples before and after ion exchange treatment. The Raman spectrum of Li_2MnO_3 phase contains seven main peaks, which are located at 614, 568, 492, 438, 372, 334, 246 cm^{-1}. The peak positions are in good agreement with the reported values [30]. The Raman spectrum of $Li_xNi_{1/3}Mn_{2/3}O_2$ shows two main sharp peaks located at 608, 490 cm^{-1} and two weak peaks located at 435, 374 cm^{-1}. Similar Raman spectra have been observed for $Li_{1.2}Ni_{0.175}Co_{0.1}Mn_{0.52}O_2$ solid solution [31]. Also, the detectable Raman peaks of $Li_xNi_{1/3}Mn_{2/3}O_2$ become broad compared to those of Li_2MnO_3. The broadening of Raman lines would be attributed to the existence of a cationic disorder due to the nature of the stacking faults. The Raman results are in broad agreement with that of FTIR, which also suggests that $Li_xNi_{1/3}Mn_{2/3}O_2$ might exhibit similar cationic environment as that of Li_2MnO_3.

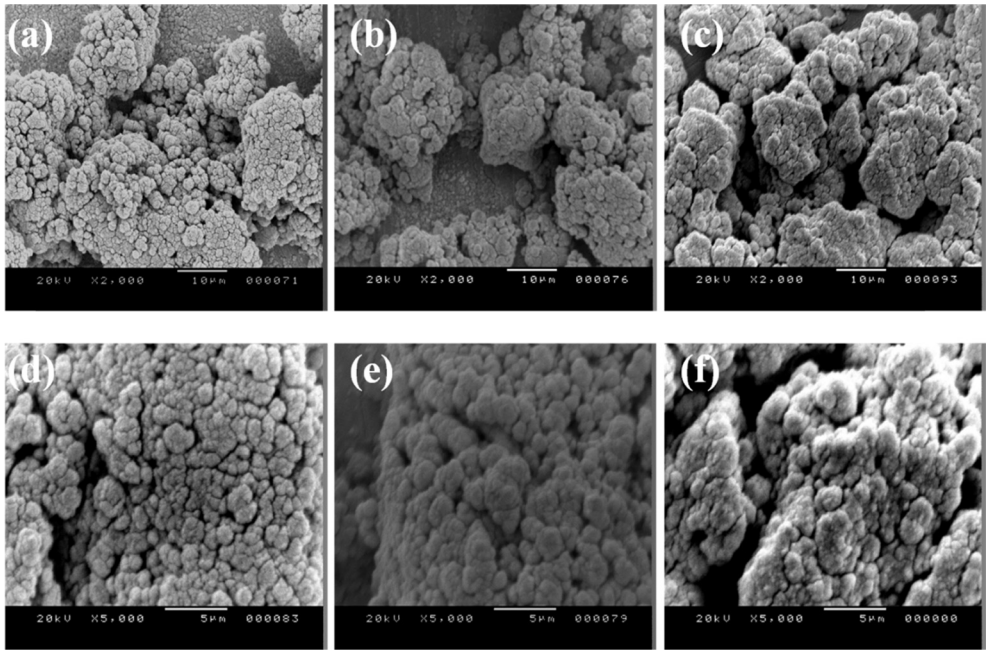

Fig. 2. SEM images P3 precursor (a) and (d), normal ion exchanged $Li_{2/3}Ni_{1/3}Mn_{2/3}O_2$ (b) and (e) and $Li_xNi_{1/3}Mn_{2/3}O_2$ (c) and (f).

Galvanostatic charge–discharge profiles of two ion exchanged samples measured at 50 °C are shown in Fig. 5. The measurements were carried out between 4.7 V and 2.5 V with a current density of 20 mA g^{-1} (0.1 C rate). $Li_{2/3}Ni_{1/3}Mn_{2/3}O_2$ shows typical charge–discharge profiles as those of reported before [32]. Since only 1/3 mol Li can be extracted from $Li_{2/3}Ni_{1/3}Mn_{2/3}O_2$, the first discharge capacity of $Li_{2/3}Ni_{1/3}Mn_{2/3}O_2$ is larger than the charge capacity. The reversible voltage plateau at around 3 V originates from the Mn^{4+}/Mn^{3+} redox couple. In contrast, $Li_xNi_{1/3}Mn_{2/3}O_2$ cathode exhibits different charge–discharge profiles. During charging of $Li_xNi_{1/3}Mn_{2/3}O_2$ cathode, there is a gradual increase in capacity against potential below 4.5 V. The charge capacity in this range is found to be around 110 mAh g^{-1}, which is in good agreement with the capacity contributed to Ni^{2+}/Ni^{3+} or Ni^{2+}/Ni^{4+} redox couples. When the cathode is charged above 4.5 V, voltage plateau can be observed. This plateau only appears at the first charge cycle and vanishes in the following cycles. This charge–discharge behavior is characteristic feature for lithium-excess manganese metal oxide, xLi_2MnO_3–$(1-x)$ $LiMO_2$ (M = Mn, Ni, Co, Fe). The irreversible plateau observed at around 4.5 V has been demonstrated to be due to the extraction of Li from Li layer together with the oxygen release from the electrode [22,33]. As it was proved by the XRD measurement, $Li_xNi_{1/3}Mn_{2/3}O_2$ prepared from this method show similar XRD patterns to that of lithium-excess manganese metal oxides.

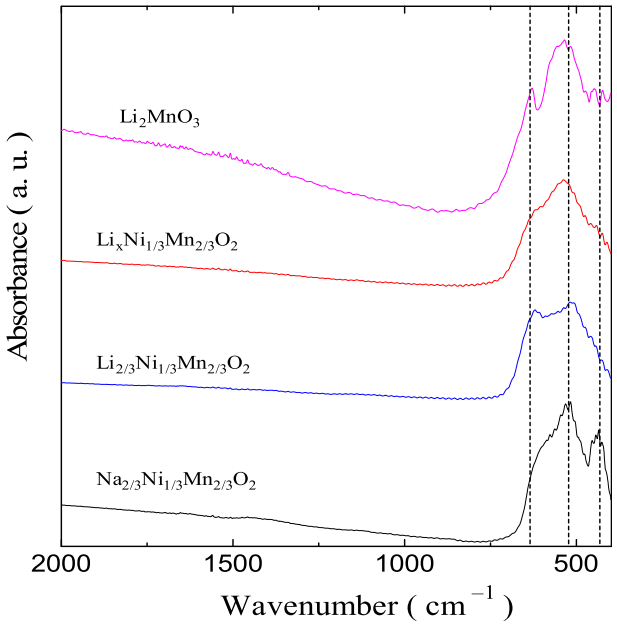

Fig. 3. FTIR spectra of Li_2MnO_3, P3 precursors and ion exchanged samples.

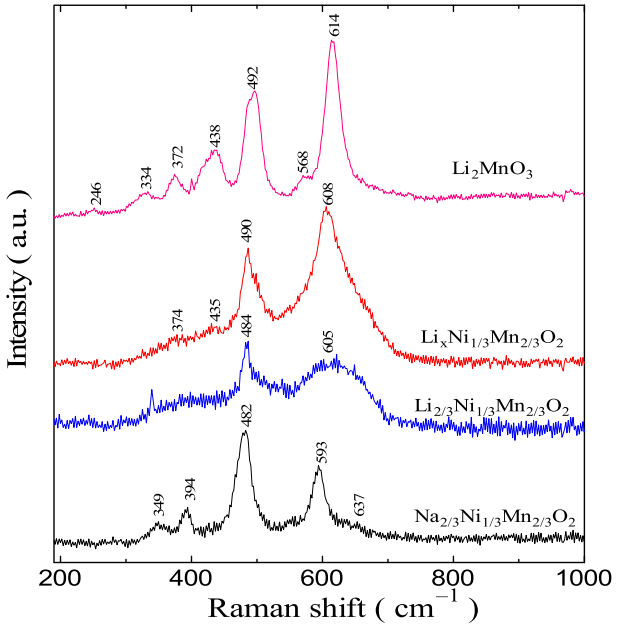

Fig. 4. Raman spectra of Li_2MnO_3, P3 precursors and ion exchanged samples.

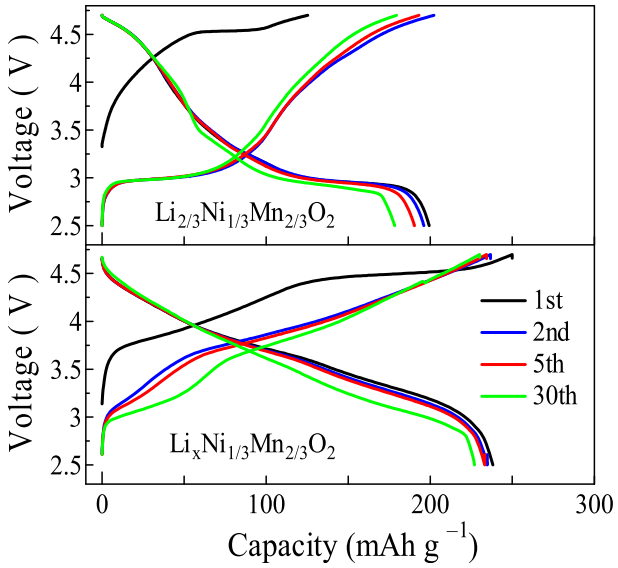

Fig. 5. Galvanostatic charge–discharge profiles of two ion exchanged samples measured at 50 °C.

Therefore, it is reasonable to obtain similar charge–discharge profiles as those of lithium-excess manganese metal oxides. However, different from the common lithium-excess manganese metal oxide which shows large irreversible capacity, $Li_xNi_{1/3}Mn_{2/3}O_2$ prepared in this study exhibits very small irreversible capacity (around 11 mAh g^{-1}) and high first cycle efficiency. The first charge capacity of $Li_xNi_{1/3}Mn_{2/3}O_2$ is 249.9 mAh $/g^{-1}$ and the initial cycle efficiency can reach as high as 95.3%. The initial cycle efficiency is higher than the reported Li_2MnO_3 [34] and lithium-excess manganese metal oxides [22,35]. The capacity retention after 30 cycles also keeps at 95.6%, which indicates good cycle performance of $Li_xNi_{1/3}Mn_{2/3}O_2$ cathode. In addition to low irreversible capacity and high capacity retention, one can see that most of the reversible capacity for $Li_xNi_{1/3}Mn_{2/3}O_2$ cathode is delivered above 3 V compared to $Li_{2/3}Ni_{1/3}Mn_{2/3}O_2$ cathode. This suggests that high energy density for $Li_xNi_{1/3}Mn_{2/3}O_2$ can be obtained since its high operating voltage. The enhanced first cycle charge efficiency and better stability of our electrode materials would be contributed to several factors. One possible reason might be due to the existence of oxygen deficiency in the electrode material prepared from reduction-ion exchanged. The effect of oxygen deficiency in Li_2MnO_3 cathode material has been studied by Kubota et al. [36]. In their study, oxygen deficient Li_2MnO_3 also showed improved first charging efficiency and better cyclic stability. However, more advanced structural analysis techniques are necessary to clarify the reason for the improved electrochemical performance of $Li_xNi_{1/3}Mn_{2/3}O_2$ electrode material.

Table 2
Lattice parameters of $Na_{2/3}Ni_{1/3}Mn_{2/3}O_2$ and its metal substituted samples.

Sample	Lattice parameters		
	a (Å)	c (Å)	V (Å^3)
$Na_{2/3}Ni_{1/3}Mn_{2/3}O_2$	2.879	16.721	120.04
$Na_{2/3}Ni_{2/9}Mg_{1/9}Mn_{2/3}O_2$	2.886	16.766	121.02
$Na_{2/3}Ni_{2/9}Al_{1/9}Mn_{2/3}O_2$	2.873	16.824	120.30
$Na_{2/3}Ni_{2/9}Fe_{1/9}Mn_{2/3}O_2$	2.885	16.799	121.12
$Na_{2/3}Ni_{2/9}Co_{1/9}Mn_{2/3}O_2$	2.864	16.779	119.21

3.2. Characterization of metal ions substituted $Li_xNi_{2/9}M_{1/9}Mn_{2/3}O_2$ (M = Al, Co, Fe, Mg)

Since we have succeeded in preparing $Li_xNi_{1/3}Mn_{2/3}O_2$ cathode with good electrochemical properties, it would be of great interest to further investigate the effect of foreign metal substitution for Ni. Fig. 6 shows the XRD profiles of P3 precursors. All peaks in the XRD patterns of precursors can be indexed to P3 layer structure with no impurities. The XRD patterns of metal submitted show the same pattern as that of $Na_{2/3}Ni_{1/3}Mn_{2/3}O_2$, which indicates that partial substitution of Ni by other foreign metal ions does not affect the main structure of $Na_{2/3}Ni_{1/3}Mn_{2/3}O_2$. This observation is consistent with the metallic metal elements doped P2 $Na_{2/3}Ni_{1/3}Mn_{2/3}O_2$ reported by Komaba et al. [37]. It is believed that the difference in metal ion radius may result in the change in the lattice parameters of the precursors. Therefore, in order to study the effect ion radius

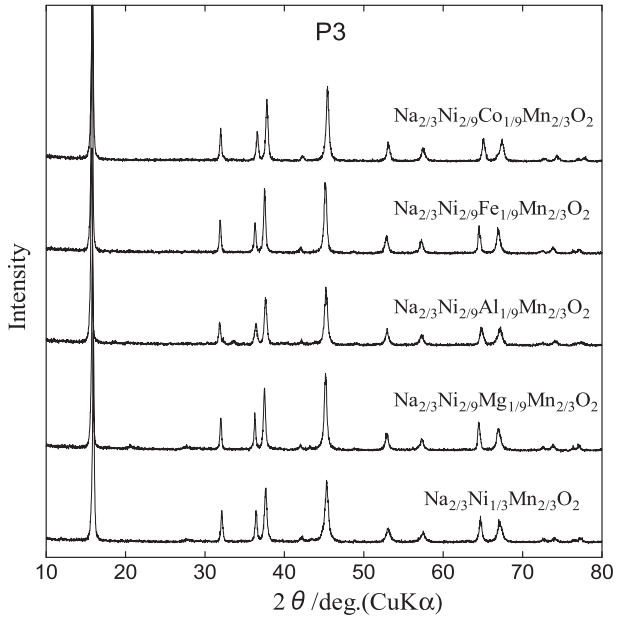

Fig. 6. XRD profiles of P3 $Na_{2/3}Ni_{1/3}Mn_{2/3}O_2$ and its metal substituted samples.

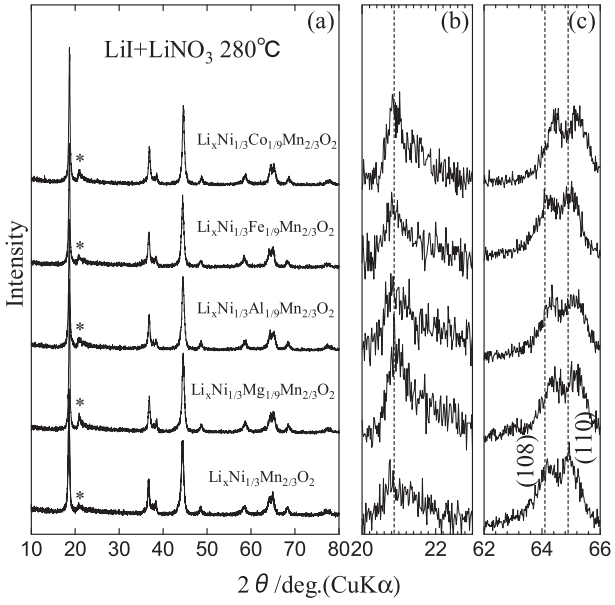

Fig. 7. XRD patterns of ion exchanged samples.

Table 3
Lattice parameters of ion exchange samples.

Samples	Lattice parameters		
	a (Å)	*c* (Å)	*V* (Å^3)
$Li_xNi_{1/3}Mn_{2/3}O_2$	2.866	14.278	101.598
$Li_xNi_{2/9}Mg_{1/9}Mn_{2/3}O_2$	2.863	14.239	101.054
$Li_xNi_{2/9}Al_{1/9}Mn_{2/3}O_2$	2.861	14.257	101.090
$Li_xNi_{2/9}Fe_{1/9}Mn_{2/3}O_2$	2.864	14.292	101.536
$Li_xNi_{2/9}Co_{1/9}Mn_{2/3}O_2$	2.853	14.253	100.649

of foreign metal on the structure of $Na_{2/3}Ni_{1/3}Mn_{2/3}O_2$, the lattice parameters of $Na_{2/3}Ni_{1/3}Mn_{2/3}O_2$ precursor and metal substituted samples were listed in Table 2.

The *a* and *c* axis of un-substituted $Na_{2/3}Ni_{1/3}Mn_{2/3}O_2$ is 2.879 Å and 16.721 Å, respectively. The, *a*, *c* axis, as well as cell volume of $Na_{2/3}Ni_{2/9}Mg_{1/9}Mn_{2/3}O_2$ and $Na_{2/3}Ni_{2/9}Fe_{1/9}Mn_{2/3}O_2$ increase. This can be explained by the difference in ionic radii since Mg^{2+} (0.72 Å) and Fe^{3+} (0.645 Å) have larger ionic radii than the average radii of Ni^{2+} (0.690 Å) and Mn^{4+} (0.530 Å). Similarly, *a*, *c* axis and cell volume of $Na_{2/3}Ni_{2/9}Al_{1/9}Mn_{2/3}O_2$ and $Na_{2/3}Ni_{2/9}Co_{1/9}Mn_{2/3}O_2$ decrease due to the smaller ionic radii of Al^{3+} (0.535 Å) and Co^{3+} (0.545 Å) compared to Ni^{2+} (0.690Å). This good agreement between the lattice parameter and ionic radii indicates that Ni is successfully substituted by the above elements.

The XRD patterns of ion exchanged samples are shown in Fig. 7(a). Additionally, the enlarged XRD patterns in regions 20–24° and 62–66° are presented in Fig. 7(b) and (c), respectively. All the peaks in the ion exchanged samples are indexed to O3 structure with the space group of $R\bar{3}m$. From the enlarged XRD patterns shown in Fig. 7(b) one can see the appearance of this superlattice peaks in all ion exchange samples though the peaks intensity and sharpness wary with samples. The splitting of peaks at $2\theta = 64°$ which indicates the well-defined layer structure are shown in Fig. 7(c).

Lattice parameters of ion exchange samples are summarized in Table 3. We have confirmed that the lithium ion content of metal substituted samples shows nearly same value as that of $Li_xNi_{1/3}Mn_{2/3}O_2$. Further, the shrinking in both *c* axis and cell volume can be observed for $Li_xNi_{2/9}M_{1/9}Mn_{2/3}O_2$ samples. The almost identical XRD patterns of $Li_xNi_{1/3}Mn_{2/3}O_2$ and $Li_xNi_{2/9}M_{1/9}Mn_{2/3}O_2$ suggests that

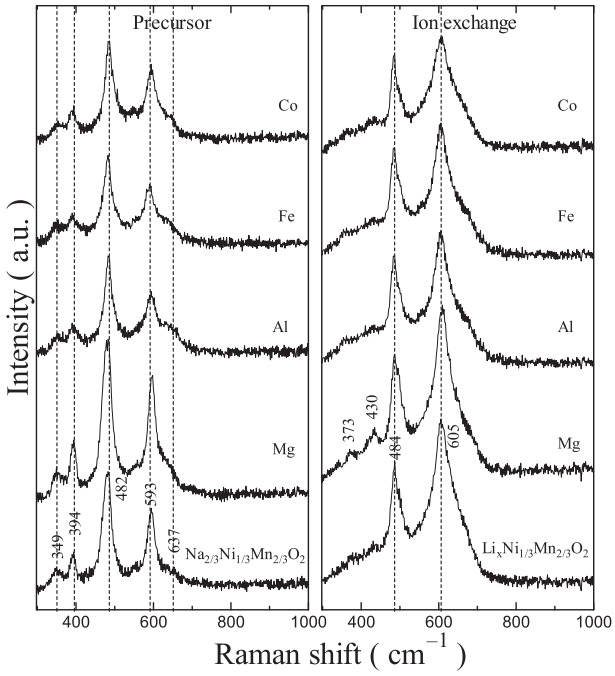

Fig. 9. Raman spectra of P3 precursors and their ion exchanged samples.

the small amount substitution of Ni with foreign metallic elements barely affects the main structure. As is pointed out by Komaba et al., small amount dope of metallic element for O3 has little effect on the structure of due to its thermo dynamical stability [37].

TEM images of $Li_xNi_{1/3}Mn_{2/3}O_2$ and $Li_xNi_{2/9}M_{1/9}Mn_{2/3}O_2$ samples are presented in Fig. 8. Faced and polygonal-shaped particles with nearly flat surface can also be observed Fig. 8(a). The primary particle size for $Li_xNi_{1/3}Mn_{2/3}O_2$ is approximately 100–250 nm. There is almost no apparent difference in the primary particle before and after metallic element substituted as observed from the TEM images. This result reveals that mall amount substitution of metallic element for Ni seemed to have little effect on the primary particle size.

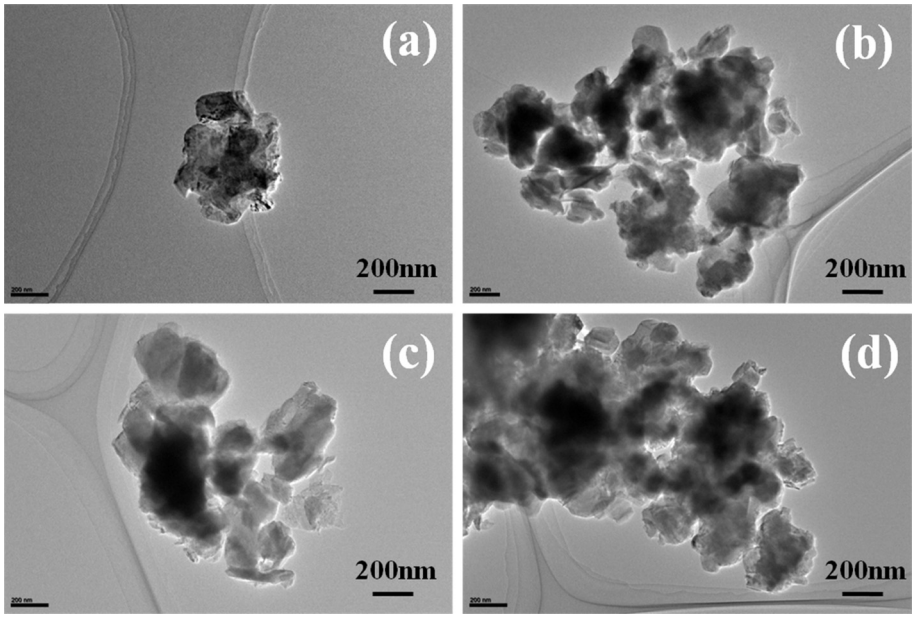

Fig. 8. TEM images of $Li_xNi_{1/3}Mn_{2/3}O_2$ and metal substituted ion exchanged samples. (a) $Li_xNi_{1/3}Mn_{2/3}O_2$, (b) $Li_xNi_{2/9}Mg_{1/9}Mn_{2/3}O_2$, (c) $Li_xNi_{2/9}Fe_{1/9}Mn_{2/3}O_2$, (d) $Li_xNi_{2/9}Co_{1/9}Mn_{2/3}O_2$.

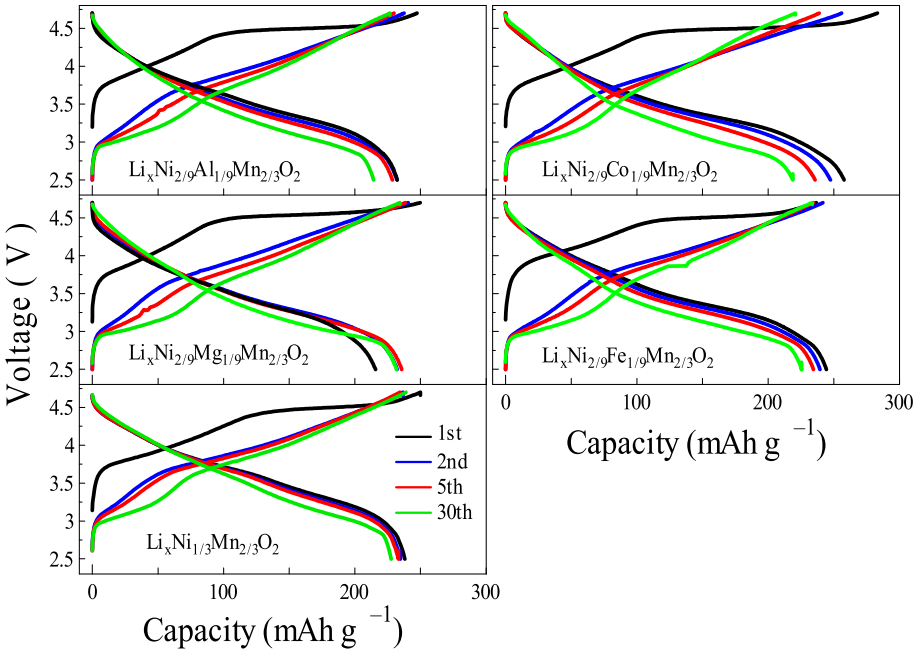

Fig. 10. Galvanostatic charge–discharge profiles of $Li_xNi_{1/3}Mn_{2/3}O_2$ and metal substituted ion exchanged samples.

Even though all the samples show similar XRD patterns, it is hard to confirm their short-range structure from XRD results. Thus, Raman spectroscopy has been employed to further evaluate the possible effect of metallic element substitution on the local structure of $LiNi_{1/3}Mn_{2/3}O_2$. The obtained Raman spectra are shown in Fig. 9. Four sharp peaks located at 349, 394, 482 and 593 cm^{-1} can be characterized to P3 $Na_{2/3}Ni_{1/3}Mn_{2/3}O_2$ as discussed above. From the Raman spectra one can see that all the metallic metal element substituted precursors display almost the same spectrum as that of pristine $Na_{2/3}Ni_{1/3}Mn_{2/3}O_2$. Through further observation it is clear that the peaks in spectrum of Mg substituted sample are in high intensity than the other samples. In the case of ion exchanged sample, almost same trend is observed as for the precursors. For Mg substituted sample, $Li_xNi_{2/9}Mg_{1/9}Mn_{2/3}O_2$, Raman peaks located at 373 and 430 cm^{-1} become predominant. The relatively well defined Raman peaks of $Li_xNi_{2/9}Mg_{1/9}Mn_{2/3}O_2$ suggest the good crystallization and well growth integrity of the layered structure.

The voltage profiles of the samples are shown in Fig. 10. Metal ions substituted samples show similar voltage–capacity profile as those of $Li_xNi_{1/3}Mn_{2/3}O_2$. The first charge capacity, discharge capacity, initial cycle efficiency and capacity retention after 30 cycles are summarized in Table 4. Except for $Li_xNi_{2/9}Co_{1/9}Mn_{2/3}O_2$, one can see that the first charge capacity for other metal ions substituted samples is nearly same as that of un-substituted $Li_xNi_{1/3}Mn_{2/3}O_2$. In the case of Al and Fe substituted samples, both of them show improved initial cycle efficiency compared to $Li_xNi_{1/3}Mn_{2/3}O_2$. The first charge capacity of Co substituted sample is 283.1 mAh g^{-1}, which value is much higher than that of pristine $Li_xNi_{1/3}Mn_{2/3}O_2$. However, the capacity retention after 30 cycles is 84.6%. For Mg substituted sample, extremely high capacity retention after 30 cycles is obtained even though the initial cycle efficiency is lower than those of the other samples. From the above discussion it was found that $Li_xNi_{2/9}Mg_{1/9}Mn_{2/3}O_2$ shows good crystallization and well growth integrity of the layered structure. Also, it is reported that Mg might occupy both the Li and transition metal sites [38]. Mg present in the Li layer would tend to stabilize the structure during charge-and discharge cycling.

Cycle performance of ion exchanged samples at 50 °C is presented in Fig. 11. The capacity of Co substituted cathode decreases rapidly in the first several cycles and continues to decrease upon cycling. For Al and Fe substituted cathodes, although there is rapid decay in capacity at the initial 5 cycles, they still exhibit relatively stable capacity retention upon further cycling. One can observe that substitution with Mg gives the best cycle performance compared to the other samples. The possible reason for the improved cycleability of Mg substituted cathode would be due to stabilization of the structure. Fig. 12 displays the rate capability of various ion exchanged samples. All the cathodes were cycled in the voltage range of 2.5–4.7 V at 50 °C with various current density. One can see that $Li_xNi_{2/9}Co_{1/9}Mn_{2/3}O_2$ displays higher capacity than those of other cathodes at the initial several cycles. This could be contributed to the elevated conductivity of $Li_xNi_{1/3}Mn_{2/3}O_2$ after Co substitution. However, the capacity at higher current density drops and becomes lower than pristine $Li_xNi_{1/3}Mn_{2/3}O_2$, which might be due to the capacity fading at prolonged cycles. For $Li_xNi_{2/9}Mg_{1/9}Mn_{2/3}O_2$, the capacity increase gradually at the first several cycles and delivers good rate capability compared with the other samples.

Table 4
1st charge and discharge capacity, charge efficiency and capacity retention of ion exchanged samples.

Samples	1st charge capacity (mAh g^{-1})	1st discharge capacity (mAh g^{-1})	Charge efficiency (%)	Capacity retention after 30 cycles (%)
$Li_xNi_{1/3}Mn_{2/3}O_2$	249.9	238.1	95.3	95.6
$Li_xNi_{2/9}Mg_{1/9}Mn_{2/3}O_2$	249.8	220.0	92.7	105.3
$Li_xNi_{2/9}Al_{1/9}Mn_{2/3}O_2$	247.3	236.6	95.7	95.3
$Li_xNi_{2/9}Fe_{1/9}Mn_{2/3}O_2$	249.2	244.3	98.0	92.5
$Li_xNi_{2/9}Co_{1/9}Mn_{2/3}O_2$	283.1	257.8	91.0	84.6

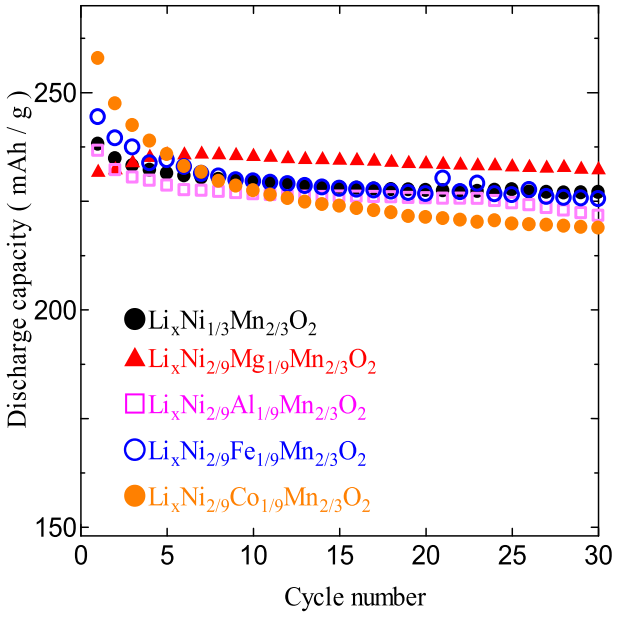

Fig. 11. Cycle performance of $Li_xNi_{1/3}Mn_{2/3}O_2$ and metal ions substituted samples.

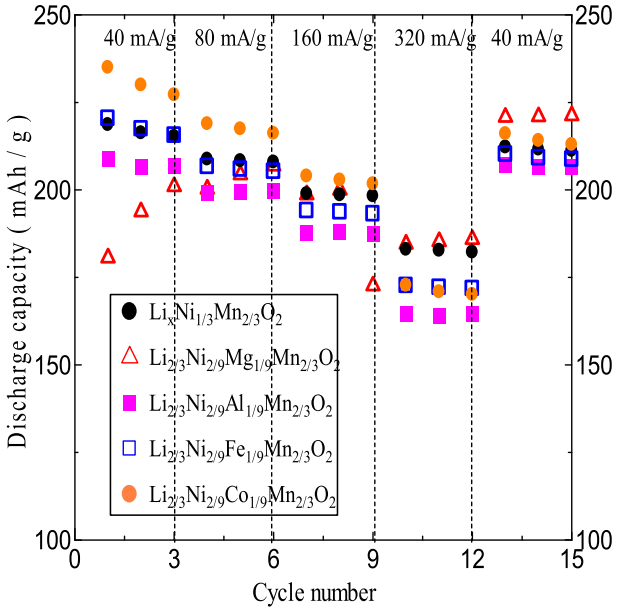

Fig. 12. Rate capability of $Li_xNi_{1/3}Mn_{2/3}O_2$ and metal ions substituted samples.

4. Conclusions

A new synthesis procedure has been developed to obtain Li_2MnO_3 related cathode materials via a simultaneous reduction-ion exchange of P3 type $Na_{2/3}Ni_{1/3}Mn_{2/3}O_2$. Compared with the samples prepared from conventional ion exchange method, extra Li, more than 1/3 mol, were successfully incorporated in $Li_{2/3}Ni_{1/3}Mn_{2/3}O_2$ matrix to form $Li_xNi_{1/3}Mn_{2/3}O_2$ under a simultaneous reduction with LiI. The as prepared $Li_xNi_{1/3}Mn_{2/3}O_2$ showed almost the same XRD patterns and similar cationic environment as that of Li-excess manganese oxide based cathode materials. From the galvanostatic charge–discharge curves it was found that $Li_xNi_{1/3}Mn_{2/3}O_2$ cathode exhibited Li_2MnO_3 type potential–capacity profiles. Furthermore, $Li_xNi_{1/3}Mn_{2/3}O_2$ cathode showed small irreversible capacity and improved cycleability. The XRD, FTIR and Raman results of $Li_xNi_{2/9}M_{1/9}Mn_{2/3}O_2$ suggested that partially substitution of Ni with other foreign metal ions seemed to have little effect on the structure of $Li_xNi_{1/3}Mn_{2/3}O_2$. Mg substituted cathode showed improved cycleability as well as rate capability compared to other metal ions substituted samples. It was considered that Mg substitution could be beneficial for stabilizing the $LiMnO_2$ structure thereby leads to improved electrochemical properties. Our study demonstrates that the simultaneous reduction-ion exchange method can be used to prepare Li-excess manganese based cathode material with enhanced first cycle efficiency and cycleability.

References

[1] A.R. Armstrong, P.G. Bruce, Nature 381 (1996) 499–500.
[2] P.G. Bruce, A.R. Armstrong, R. Gitzendanner, J. Mater. Chem. 9 (1999) 193–198.
[3] R.J. Gummow, A. de Kock, M.M. Thackeray, Solid State Ionics 69 (1994) 59–67.
[4] Y.J. Park, J.G. Kim, M.K. Kim, H.T. Chung, W.S. Um, M.H. Kim, H.G. Kim, J. Power Sources 76 (1998) 41–47.
[5] M.M. Doeff, M.Y. Peng, Y. Ma, L.C. De Jonghe, J. Electrochem. Soc. 141 (1994) L145–L147.
[6] J. Akimoto, J. Awaka, Y. Takahashi, N. Kijima, M. Tabuchi, A. Nakashima, H. Sakaebe, K. Tatsumi, Electrochem. Solid State Lett. 8 (2005) A554–A557.
[7] J. Awaka, J. Akimoto, H. Hayakawa, Y. Takahashi, N. Kijima, M. Tabuchi, H. Sakaebe, K. Tatsumi, J. Power Sources 174 (2007) 1218–1223.
[8] A.D. Robertson, A.R. Armstrong, A.J. Fowkes, P.G. Bruce, J. Mater. Chem. 11 (2001) 113–118.
[9] G. Vitins, K. West, J. Electrochem. Soc. 144 (1997) 2587–2592.
[10] A.R. Armstrong, R. Gitzendanner, A.D. Robertson, P.G. Bruce, Chem. Commun. (1998) 1833–1834.
[11] C.S. Johnson, J. Power Sources 165 (2007) 559–565.
[12] M.M. Thackeray, S.H. Kang, C.S. Johnson, J.T. Vaughey, R. Benedek, S.A. Hackney, J. Mater. Chem. 17 (2007) 3112–3215.
[13] M. Tabuchi, A. Nakashima, K. Ado, H. Sakaebe, H. Kobayashi, H. Kageyama, K. Tatsumi, Y. Kobayashi, S. Seki, A. Yamanaka, J. Power Sources 146 (2005) 287–293.
[14] M. Tabuchi, Y. Nabeshima, T. Takeuchi, K. Tatsumi, J. Imaizumi, Y. Nitta, J. Power Sources 195 (2010) 834–844.
[15] C. Delmas, C. Braconnier, P. Hagenmuller, Mater. Res. Bull. 17 (1982) 117–123.
[16] A. Mendiboure, C. Delmas, P. Hagenmuller, Mater. Res. Bull. 19 (1984) 1383–1392.
[17] C. Delmas, I. Saadoune, Solid State Ionics 53 (1992) 370–375.
[18] J.M. Paulsen, C.L. Thomas, J.R. Dahn, J. Electrochem. Soc. 146 (1999) 3560–3565.
[19] J.M. Paulsen, J.R. Dahn, Solid State Ionics 126 (1999) 3–24.
[20] J.M. Paulsen, C.L. Thomas, J.R. Dahn, J. Electrochem. Soc. 147 (2000) 861–869.
[21] J.M. Paulsen, J.R. Dahn, J. Electrochem. Soc. 147 (2000) 2478–2485.
[22] D. Mohanty, S. Kalnaus, R. Meisner, K.J. Rhodes, J. Power Sources 229 (2013) 239–248.
[23] J.M. Tarascon, D. Guyomard, J. Electrochem. Soc. 138 (1991) 2864–2868.
[24] M.H. Rossouw, D.C. Liles, M.M. Thackeray, J. Solid State Chem. 104 (1993) 464–466.
[25] M. Unno, T. Kikukawa, M. Kumauchi, N. Kamo, J. Phys. Chem. B 117 (2013) 1321–1325.
[26] T. Shingae, K. Kubota, M. Kumauchi, F. Tokunaga, M. Unno, J. Phys. Chem. Lett. 4 (2013) 1322–1327.
[27] K.M. Shaju, G.V. Subba Rao, B.V.R. Chowdari, Electrochem. Commun. 4 (2002) 633–638.
[28] C.M. Julien, Ionics 6 (2000) 30–46.
[29] C.M. Burba, R. Frech, Electrochim. Acta 52 (2006) 780–785.
[30] C.M. Julien, M. Massot, Mater. Sci. Eng. B 100 (2003) 69–78.
[31] G. Singh, W.C. West, J. Soler, R.S. Katiyar, J. Power Sources 218 (2012) 34–38.
[32] D. Pasero, N. Reeves, L. Gillie, V. Pralong, A.R. West, J. Electrochem. Soc. 154 (2007) A760–A769.
[33] N. Yabuuchi, K. Yoshii, S.T. Myung, I. Nakai, S. Komaba, J. Am. Chem. Soc. 133 (2011) 4404–4419.
[34] Y.W. Denis, K. Yanagida, Y. Kato, H. Nakamura, J. Electrochem. Soc. 156 (2009) A417–A424.
[35] J.M. Zheng, X.B. Wu, Y. Yang, Electrochim. Acta 56 (2011) 3071–3078.
[36] K. Kubota, T. Kaneko, M. Hirayama, M. Yonemura, Y. Imanari, K. Nakane, R. Kanno, J. Power Sources 216 (2012) 249–255.
[37] S. Komaba, K. Yoshii, A. Ogata, I. Nakai, Electrochim. Acta 54 (2009) 2353–2359.
[38] P. Suresh, A.K. Shukla, N. Munichandran, J. Electrochem. Soc. 153 (2005) 2273–2280.